First results of the Instrumentation Line for the deep-sea ANTARES neutrino telescope

J.A. Aguilar[j], A. Albert[u], F. Ameli[x], M. Anghinolfi[i], G. Anton[g], S. Anvar[y], E. Aslanides[e], J-J. Aubert[e], E. Barbarito[b], S. Basa[r], M. Battaglieri[i], Y. Becherini[c], R. Bellotti[b], J. Beltramelli[y], V. Bertin[e], A. Bigi[w], M. Billault[e], R. Blaes[u], N. de Botton[y], M.C. Bouwhuis[v], S.M. Bradbury[t], R. Bruijn[v,ab], J. Brunner[e], G.F. Burgio[f], J. Busto[e], F. Cafagna[b], L. Caillat[e], A. Calzas[e], A. Capone[x], L. Caponetto[f], E. Carmona[j], J. Carr[e], S.L. Cartwright[z], D. Castel[u], E. Castorina[w], V. Cavasinni[w], S. Cecchini[c,m], A. Ceres[b], P. Charvis[h], P. Chauchot[k], T. Chiarusi[x], M. Circella[b], C. Colnard[v], C. Compère[k], R. Coniglione[s], N. Cottini[w], P. Coyle[e], S. Cuneo[i], A-S. Cussatlegras[d], G. Damy[k], R. van Dantzig[v], C. De Marzo[b 1], I. Dekeyser[d], E. Delagnes[y], D. Denans[y], A. Deschamps[h], F. Dessages-Ardellier[y], J-J. Destelle[e], B. Dinkespieler[e], C. Distefano[s], C. Donzaud[y], J-F. Drogou[ℓ], F. Druillole[y], D. Durand[y], J-P. Ernenwein[u], S. Escoffier[e], E. Falchini[w], S. Favard[e], F. Feinstein[e], S. Ferry[n], D. Festy[k], C. Fiorello[b], V. Flaminio[w], S. Galeotti[w], J-M. Gallone[n], G. Giacomelli[c], N. Girard[u], C. Gojak[e], Ph. Goret[y], K. Graf[g], G. Hallewell[e], M.N. Harakeh[q], B. Hartmann[g], A. Heijboer[v,ab], E. Heine[v], Y. Hello[h], J.J. Hernández-Rey[j], J. Hößl[g], C. Hoffman[n], J. Hogenbirk[v], J.R. Hubbard[y], M. Jaquet[e], M. Jaspers[v,ab], M. de Jong[v], F. Jouvenot[y], N. Kalantar-Nayestanaki[q], A. Kappes[g], T. Karg[g], S. Karkar[e], U. Katz[g], P. Keller[e], H. Kok[v], P. Kooijman[v,aa], C. Kopper[g], E.V. Korolkova[z], A. Kouchner[a], W. Kretschmer[g], A. Kruijer[v], S. Kuch[g], V.A. Kudryavstev[z], D. Lachartre[y], H. Lafoux[y], P. Lagier[e], R. Lahmann[g], G. Lamanna[e], P. Lamare[y], J.C. Languillat[y], H. Laschinsky[g], Y. Le Guen[k], H. Le Provost[y], A. Le Van Suu[e], T. Legou[e], G. Lim[v,ab], L. Lo Nigro[f], D. Lo Presti[f],

H. Loehner [q], S. Loucatos [y], F. Louis [y], F. Lucarelli [x], V. Lyashuk [p], M. Marcelin [r], A. Margiotta [c], R. Masullo [x], F. Mazéas [k], A. Mazure [r], J.E. McMillan [z], R. Megna [b], M. Melissas [e], E. Migneco [s], A. Milovanovic [t], M. Mongelli [b], T. Montaruli [b], M. Morganti [w], L. Moscoso [y,a], M. Musumeci [s], C. Naumann [g], M. Naumann-Godo [g], V. Niess [e], C. Olivetto [n], R. Ostasch [g], N. Palanque-Delabrouille [y], P. Payre [e], H. Peek [v], C. Petta [f], P. Piattelli [s], J-P. Pineau [n], J. Poinsignon [y], V. Popa [c,o], T. Pradier [n], C. Racca [n], N. Randazzo [f], J. van Randwijk [v], D. Real [j], B. van Rens [v], F. Réthoré [e], P. Rewiersma [v 1], G. Riccobene [s], V. Rigaud [ℓ], M. Ripani [i], V. Roca [j], C. Roda [w], J.F. Rolin [k], M. Romita [b], H.J. Rose [t], A. Rostovtsev [p], J. Roux [e], M. Ruppi [b], G.V. Russo [f], F. Salesa [j], K. Salomon [g], P. Sapienza [s], F. Schmitt [g], J-P. Schuller [x], R. Shadnize [g], I. Sokalski [b], T. Spona [g], M. Spurio [c], G. van der Steenhoven [v], T. Stolarczyk [y], K. Streeb [g], D. Stubert [u], L. Sulak [e], M. Taiuti [i], C. Tamburini [d], C. Tao [e], G. Terreni [w], L.F. Thompson [z], P. Valdy [ℓ], V. Valente [x], B. Vallage [y], G. Venekamp [v], B. Verlaat [v], P. Vernin [y], R. de Vita [i], G. de Vries [v,aa], R. van Wijk [v], P. de Witt Huberts [v], G. Wobbe [g], E. de Wolf [v,ab], A-F. Yao [d], D. Zaborov [p], H. Zaccone [y], J.D. Zornoza [j], J. Zúñiga [j]

[1] Deceased.

[a] *APC – AstroParticule et Cosmologie, UMR 7164 (CNRS, Université Paris 7, CEA, Observatoire de Paris), 11, place Marcelin Berthelot, 75231 Paris Cedex 05, France*
[b] *Dipartimento Interateneo di Fisica e Sezione INFN, Via E. Orabona 4, 70126 Bari, Italy*
[c] *Dipartimento di Fisica dell'Università e Sezione INFN, Viale Berti Pichat 6/2, 40127 Bologna, Italy*
[d] *COM – Centre d'Océanologie de Marseille, CNRS/INSU et Université de la Méditerranée, 163 Avenue de Luminy, Case 901, 13288 Marseille Cedex 9, France*
[e] *CPPM – Centre de Physique des Particules de Marseille, CNRS/IN2P3 et Université de la Méditerranée, 163 Avenue de Luminy, Case 902, 13288 Marseille Cedex 9, France*
[f] *Dipartimento di Fisica ed Astronomia dell'Università e Sezione INFN, Viale Andrea Doria 6, 95125 Catania, Italy*
[g] *Friedrich-Alexander-Universität Erlangen-Nürnberg, Physikalisches Institut, Erwin-Rommel-Str. 1, D-91058 Erlangen, Germany*
[h] *GéoSciences Azur, CNRS/INSU, IRD, Université de Nice Sophia-Antipolis, Université Pierre et Marie Curie – Observatoire Océanologique de Villefranche, BP48, 2 quai de la Darse, 06235 Villefranche-sur-Mer Cedex, France*
[i] *Dipartimento di Fisica dell'Università e Sezione INFN, Via Dodecaneso 33, 16146 Genova, Italy*
[j] *IFIC – Instituto de Física Corpuscular, Edificios Investigación de Paterna, CSIC – Universitat de València, Apdo. de Correos 22085, 46071 Valencia, Spain*
[k] *IFREMER – Centre de Brest, BP 70, 29280 Plouzané, France*
[ℓ] *IFREMER – Centre de Toulon/La Seyne Sur Mer, Port Brégaillon, Chemin Jean-Marie Fritz, 83500, La Seyne sur Mer, France*
[m] *INAF-IASF, via P. Gobetti 101, 40129 Bologna, Italy*
[n] *IPHC–Institut Pluridisciplinaire Hubert Curien, Université Louis Pasteur (Strasbourg 1) et IN2P3/CNRS, 23 rue du Loess, BP 28, 67037 Strasbourg Cedex 2, France*
[o] *Institute for Space Sciences, 77125 Bucharest, Magurele, Romania*
[p] *ITEP – Institute for Theoretical and Experimental Physics, B. Cheremushkinskaya 25, 117259 Moscow, Russia*
[q] *Kernfysisch Versneller Instituut (KVI), University of Groningen, Zernikelaan 25, 9747 AA Groningen, The Netherlands*
[r] *LAM – Laboratoire d'Astrophysique de Marseille, CNRS/INSU et Université de Provence, Traverse du Siphon – Les Trois Lucs, BP 8, 13012 Marseille Cedex 12, France*
[s] *INFN – Labaratori Nazionali del Sud (LNS), Via S. Sofia 44, 95123 Catania, Italy*
[t] *School of Physics & Astronomy, University of Leeds LS2 9JT, UK*
[u] *GRPHE – Groupe de Recherche en Physique des Hautes Energies, Université de Haute Alsace, 61 Rue Albert Camus, 68093 Mulhouse Cedex, France*
[v] *Nationaal Instituut voor Kernfysica en Hoge-Energiefysica (NIKHEF), Kruislaan 409, 1098 SJ Amsterdam, The Netherlands*
[w] *Dipartimento di Fisica dell'Università e Sezione INFN, Largo B. Pontecorvo 3, 56127 Pisa, Italy*
[x] *Dipartimento di Fisica dell'Università "La Sapienza" e Sezione INFN, P.le Aldo Moro 2, 00185 Roma, Italy*
[y] *DSM/Dapnia – Direction des Sciences de la Matière, laboratoire de recherche sur les lois fondamentales de l'Univers, CEA Saclay, 91191 Gif-sur-Yvette Cedex, France*
[z] *Dept. of Physics and Astronomy, University of Sheffield, Sheffield S3 7RH, UK*

[aa] *Universiteit Utrecht, Faculteit Betawetenschappen, Princetonplein 5, 3584 CC Utrecht, The Netherlands*
[ab] *Universiteit van Amsterdam, Instituut voor Hoge-Energiefysica, Kruislaan 409, 1098 SJ Amsterdam, The Netherlands*

Abstract

In 2005, the ANTARES Collaboration deployed and operated at a depth of 2500 m a so-called Mini Instrumentation Line equipped with Optical Modules (MILOM) at the ANTARES site. The various data acquired during the continuous operation from April to December 2005 of the MILOM confirm the satisfactory performance of the Optical Modules, their front-end electronics and readout system, as well as the calibration devices of the detector. The in-situ measurement of the Optical Module time response yields a resolution better than 0.5 ns. The performance of the acoustic positioning system, which enables the spatial reconstruction of the ANTARES detector with a precision of about 10 cm, is verified. These results demonstrate that with the full ANTARES neutrino telescope the design angular resolution of better than 0.3° can be realistically achieved.

1 Introduction

The ANTARES Collaboration is building a large underwater neutrino telescope located at a depth of 2500 m in the Mediterranean Sea, offshore from Toulon in France [1]. The experiment aims to detect neutrinos with energies above 10 GeV by means of the Cherenkov light emitted in sea water by charged particles produced in neutrino interactions with the surrounding medium. Photons are recorded by a lattice of Optical Modules [2], consisting of 10" hemispherical photomultiplier tubes [3] housed in pressure resistant glass spheres, installed along a set of mooring lines. The ANTARES detector will consist of 12 lines of 25 storeys, each storey being equipped with a triplet of Optical Modules and an electronic container mounted on a titanium frame, giving thus a grand total of 900 OMs. Some storeys also support a hydrophone for acoustic positioning or an LED Optical Beacon used for time calibration. Every line is individually connected to a Junction Box by an interconnecting cable of a few hundred metres long, laid down on the sea bed. The Junction Box is itself linked to the shore station by a 40 km long electro-optical cable equipped with 48 optical fibres. Details of the ANTARES detector architecture, components and calibration devices will be found in forthcoming publications. The installation of the 12 lines of the detector has started in February 2006 with completion expected in 2007.

In Spring 2003, two prototype lines, the Prototype Sector Line (PSL) equipped with 15 Optical Modules (OMs) and the Mini Instrumentation Line (MIL)

hosting calibration and environmental measurement devices, were deployed, connected and operated for a few months at the ANTARES site. This operation allowed a demonstration of the main aspects of the design of the detector and measurements of the background counting rates in the OMs, due to bioluminescence and ^{40}K decays, over a period of about four months [4]. After the experience of the PSL and MIL lines, significant changes were made to the detector design. In parallel to the launching of the mass production of all detector elements, the ANTARES Collaboration built a new version of the Mini Instrumentation Line based on the final design of all electronics and mechanics. This line, which also includes an extra storey with three OMs, has been named the MILOM. The main objective of the MILOM operation is to provide an in-situ check of the modified detector elements and a validation of the performance of the time calibration and the acoustic positioning devices. It was also an excellent opportunity to validate the tools and procedures used during the integration and deployment of a line before their application to the first complete ANTARES detector line. Furthermore, the MILOM houses environmental instruments needed for the calibration of the detector and the monitoring of the water physical properties.

Completed in December 2004, the MILOM line was deployed on the ANTARES site [5,6], located at $42°48'\,\mathrm{N} - 6°10'\,\mathrm{E}$, in March 2005 and connected to the existing Junction Box with the Remote Operated Vehicle (ROV) Victor of IFREMER in April 2005. It has been operating since then with almost permanent shift crews from the ANTARES shore station located in La Seyne-sur-Mer. This paper highlights the main results obtained from the MILOM operation in 2005, in particular the analysis of the Optical Module signals and of the calibration device data.

2 The MILOM line

As shown in figure 1, the MILOM consists of an instrumented releasable anchor, the Bottom String Socket (BSS), and of three storeys located respectively at 100 m, 117 m and 169 m above the sea bed (the inter-storey spacings indicated in figure 1 correspond to the cable lengths). The line is maintained in an almost vertical position by two buoys located at the top.

The MILOM is equipped with four Optical Modules: a triplet of OMs on the second storey, as for a standard ANTARES optical line storey, and a single additional OM fixed on the top storey. The line also supports three intense light sources used mainly for the OM timing calibration: the Laser Beacon located on the BSS and two LED Optical Beacons attached to the bottom and top storey, respectively. In order to allow the reconstruction of the line shape geometry, the MILOM is equipped with biaxial tiltmeters and

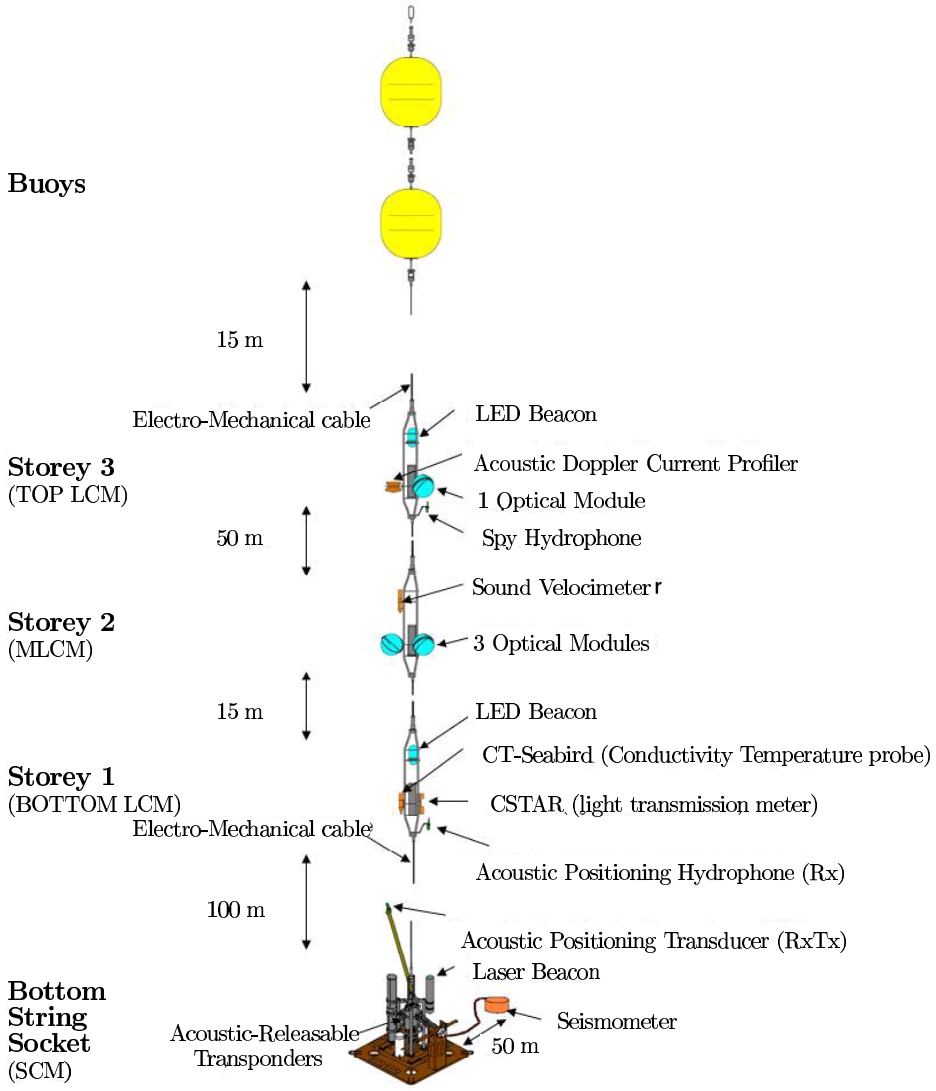

Fig. 1. Layout of the MILOM line.

compasses located in the electronics container of every storey, and with two acoustic positioning modules: an emission/reception (RxTx) module with its transducer on the BSS and a reception (Rx) module with its hydrophone on the bottom storey. In addition, the MILOM hosts various environmental devices: an acoustic current profiler [1] monitors the intensity and direction of the underwater flow; a sound velocimeter [2] records the local value of the sound

[1] 300 kHz direct reading ADCP Workhorse Monitor from Teledyne RD Instruments, http://www.rdinstruments.com/monitor.html

[2] Sound velocimeter Ref QUUX-3A(A) from Genisea/ECA, http://perso.wanadoo.fr/genisea/sound_velocimeter.htm

velocity; a CT probe [3] measures the conductivity and temperature of the sea water; a transmission meter [4] monitors the light attenuation of the water; a Spy Hydrophone records the acoustic activity from the positioning beacons, surface or biological noise; and a broadband seismometer [5] installed in the sea bed sediment 50 m away from the MILOM anchor which monitors the seismic activity at the site. Finally, the MILOM BSS is equipped with two releasable autonomous transponders [6] which enable the monitoring of the line anchor position during its deployment and allow the release of the BSS from its dead weight in order to recover the line.

All instruments deliver their data in real time and can be remotely controlled from the ANTARES shore station through a Gb Ethernet network. Every storey is equipped with a Local Control Module (LCM) which contains the electronics boards for the OM signal processing, the instrument readout, the acoustic positioning, the power system and the data transmission. On the middle storey, the Master Local Control Module (MLCM) also contains an Ethernet switch board, which multiplexes the data acquisition (DAQ) channels from the other storeys. At the bottom of the line, the BSS is equipped with a String Control Module (SCM) which contains the local readout and DAQ electronics, as well as the power system for the whole line. Finally, both MCLM and SCM include a Dense Wavelength Division Multiplexing system used for data transmission in order to merge several 1Gb/s Ethernet channels on the same pair of optical fibres by using different laser wavelengths. Although a local trigger requiring time coincidences between OMs of the same storey can be activated in each LCM, most of the time the large bandwidth of the DAQ system allows the transmission of all recorded OM signals to shore. A dedicated computer farm can then perform a global selection of the OM hits of the interesting physics events from the data recorded by the whole detector.

While the recording of the OM signals and instrument data of the MILOM started immediately after its connection, the first months of operation have been dedicated to online software development and tuning of the detector settings. The smooth data taking of the MILOM started in September 2005.

[3] MicroCAT C-T sensor SBE 37-SI from Sea Bird Electronics,
http://www.seabird.com/products/spec_sheets/37sidata.htm
[4] C-Star transmissiometer from WET Labs,
http://www.wetlabs.com/products/cstar/cstar.htm
[5] Triaxial broadband seismometer CMG-3T from Güralp Systems,
http://www.guralp.net/products/
[6] Acoustic releasable transponder RT661B2T from IXSEA,
http://www.ixsea.com/php/contenu/en/p-oceano_ocean.php

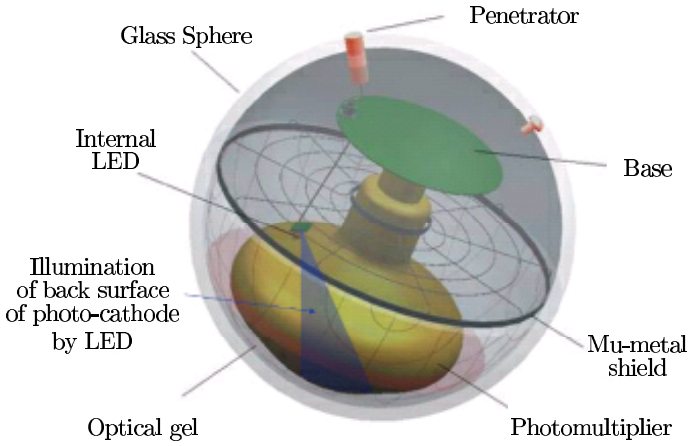

Fig. 2. Sketch of the ANTARES Optical Module (for a complete description, see ref [2]).

3 The Optical Module data

The ANTARES Optical Module consists of a 10" Hamamatsu photomultiplier tube (PMT) housed in a pressure resistant glass sphere (see figure 2). The 900 PMTs foreseen for the ANTARES detector have been selected and fully characterized to work with a threshold below the single photo-electron level with a mean transit time spread (TTS) of $\sigma \sim 1.3$ ns (FWHM ~ 3.0 ns) [3]. The PMT signal is processed by the Analogue Ring Sampler (ARS) ASIC which measures the arrival time and charge of the pulse [7]. Only this information is sent to shore in the case where it is compatible with a single photo-electron (SPE) pulse, while the ARS can perform a full digitisation of the PMT signal for larger amplitudes. In order to minimize the dead time, every OM is read out by a pair of ARS chips which treat the signal alternately according to a token ring protocol.

During normal operation, the PMT high voltage is set so as to obtain a gain of 5×10^7 leading to a SPE signal amplitude of about 45 mV. The readout trigger threshold of the ARS is set to ~ 0.5 photo-electrons. Figure 3 shows an example of the counting rates recorded by the three OMs located on the MILOM second storey over a period of 120 seconds. The counting rates exhibit a baseline largely dominated by optical background due to ^{40}K decays and bioluminescence coming from bacteria, as well as bursts of a few seconds duration produced by bioluminescent emission of macro-organisms [8]. The fourth OM located on the top storey has not worked since the beginning of the MILOM operation because it shares its power supply with a faulty Optical Beacon placed on that same storey. A visual survey of the MILOM line with the ROV Victor revealed that this Optical Beacon is full of water due to a leak.

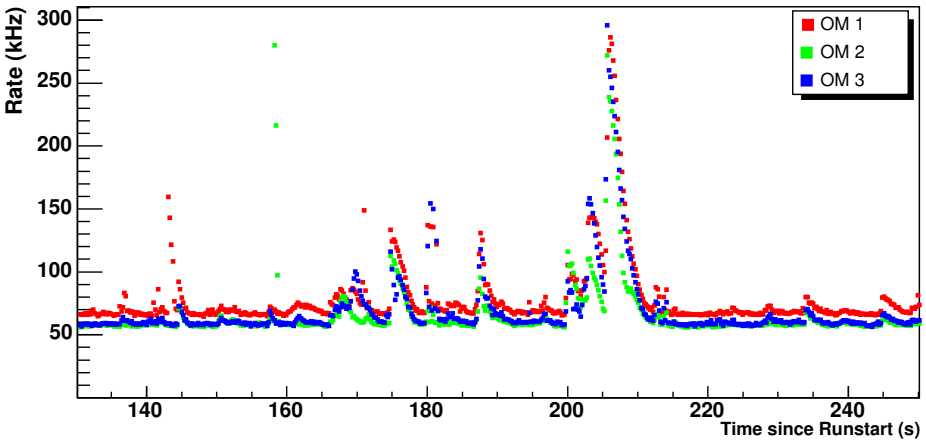

Fig. 3. Example of counting rates for the three OMs located on the second storey of the MILOM over a period of 120 seconds.

For each OM, the baseline rate is defined as the average of the minimum counting rate during periods of 15 minutes. Figure 4 shows the summary of the baseline rates extracted from the data recorded by the three OMs for a period of three months during Autumn 2005. The variability of the bioluminescence component of the baseline, already observed during the operation of the Prototype Sector Line in 2003, is confirmed by the present data. The baseline counting rates decrease from 80-90 kHz in mid-September to about 60 kHz in November 2005. Figures 3 and 4 also clearly reveal that the counting rate of one Optical Module (OM1) is systematically larger by about 15% with respect to the other two. This difference is attributed to a lower threshold value of the PMT.

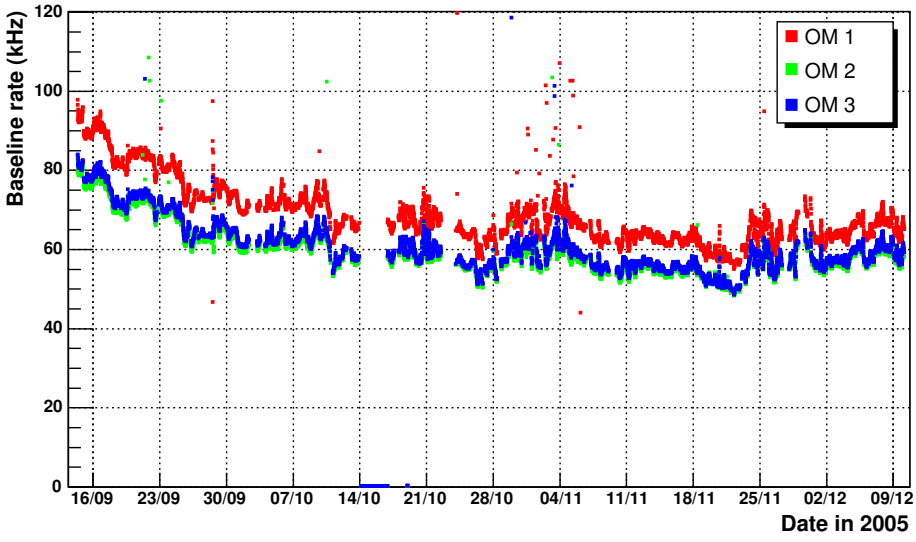

Fig. 4. Baseline rates for the three OMs during Autumn 2005.

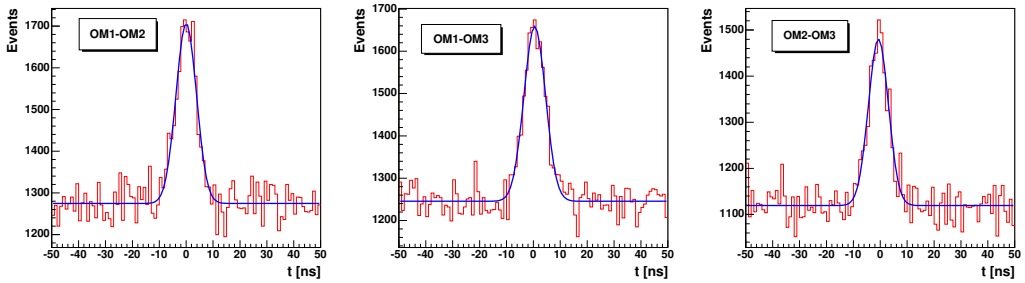

Fig. 5. Distributions of time differences between hits registered by the three OM pairs. The solid lines are fits of a Gaussian and a constant background to these distributions used to extract the ^{40}K coincidence rates.

Time coincidences between signals of OM pairs have also been studied. Figure 5 shows typical distributions of the time delay between signals from the three possible combinations. The distributions show peaks due to ^{40}K radioactive decays producing two detected photons, superimposed upon a flat background of random coincidences. The genuine ^{40}K coincidence rates obtained from fits to these distributions are 13.0 ± 0.5 Hz for the OM1-OM2 and OM1-OM3 pairs and 10.5 ± 0.4 Hz for the OM2-OM3 pair. These results are found to be stable within the statistical errors over a period of four months. The measured rates are in good agreement with a simulation of the signals induced by ^{40}K decays which leads to a coincidence rate of 12 Hz with a 4 Hz systematic error due to uncertainties in the effective area and angular response of the OMs. These measurements also confirm that the larger counting rate observed with OM1 is not due to noise in its front-end electronics.

As mentioned previously, the ARS has also the capability to perform a full waveform sampling (WF) of the OM signal in addition to the charge measurement of the PMT pulse and its arrival time. Although this functionality is mainly used to record double pulses or large amplitude signals, it is useful to cross-check the computation of the SPE charge by the integrator circuit of the ARS. In WF mode, 128 digitisations of the OM anode signal are provided, at a sampling rate of 640 MHz. In order to obtain a precise time stamping of the WF data, a synchronous sampling of the 50 MHz internal ARS clock is also performed and read out in addition to the OM data. An example of a WF record is shown in figure 6 (left). Figure 6 (middle) displays the charge distribution of the OM signals obtained by integrating the WF samples after baseline subtraction. The single photo-electron peak is clearly identified well above the electronics noise. Figure 6 (right) also shows as a comparison the charge distribution measured by the Analogue-to-Voltage converter (AVC) circuit of the ARS.

The stability of the measurements of the signal charge obtained with the integrator circuit of the ARS is shown in figure 7. This figure displays the variation of the mean charge measured by every ARS AVC circuit as a function

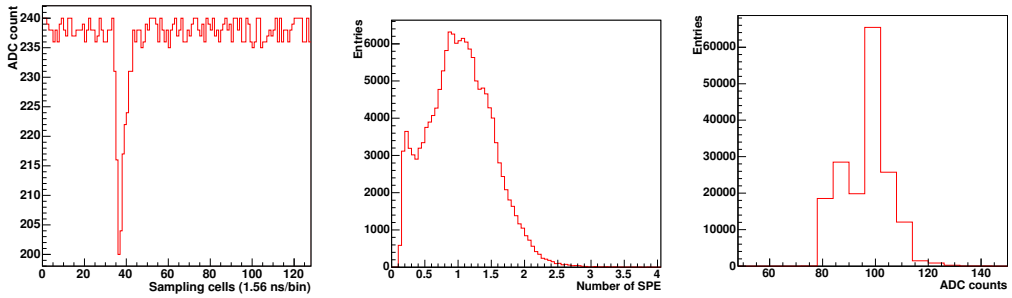

Fig. 6. Example of a waveform sampling of an OM signal (left). Charge distribution of the PMT signal obtained by integrating the WF samples (middle) and measured by the AVC circuit of the ARS (right).

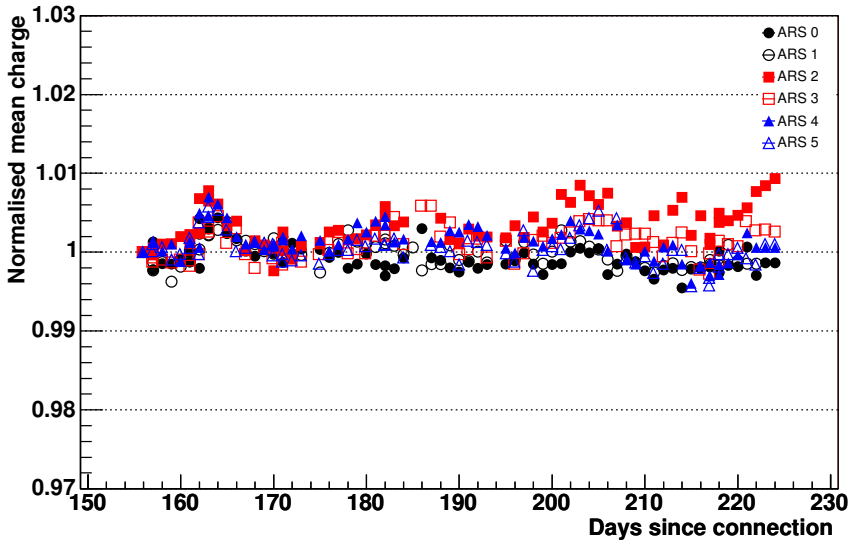

Fig. 7. Variation of the mean charge measured by the Analogue-to-Voltage converter (AVC) of every ARS as a function of time for the three OMs. The normalised mean charge is computed as the ratio between the daily mean value of the charge distribution and the mean value of their first measurement appearing in the plot.

of time for the three OMs. The normalised mean charge is computed as the ratio between the daily mean value of the charge distribution and the mean value of their first measurement appearing in the plot. This figure is obtained from the analysis of minimum bias data largely dominated by SPE events. As can be seen in figure 7, the charge distributions remain stable within $\pm 1\%$ for all ARSs during more than two months of monitoring. This indicates that the PMT gain, the trigger threshold and the charge integrators did not fluctuate by more than a few percent during that period.

4 Optical Module timing precision

The ANTARES neutrino telescope is designed to have an angular resolution of less than 0.3° for neutrino energies in excess of 10 TeV, which relies on good positioning accuracy (see section 5) and good timing resolution of the signals recorded by the Optical Modules. The specification for the timing resolution is such that it should be limited by the transit time spread of the PMTs which have $\sigma \sim 1.3$ ns and by the effect of scattering and chromatic dispersion of the light during its transmission in water, which will contribute with a similar amount to the time uncertainty. To achieve this specification, all electronics and calibration systems are required to contribute less than 0.5 ns to the overall timing resolution.

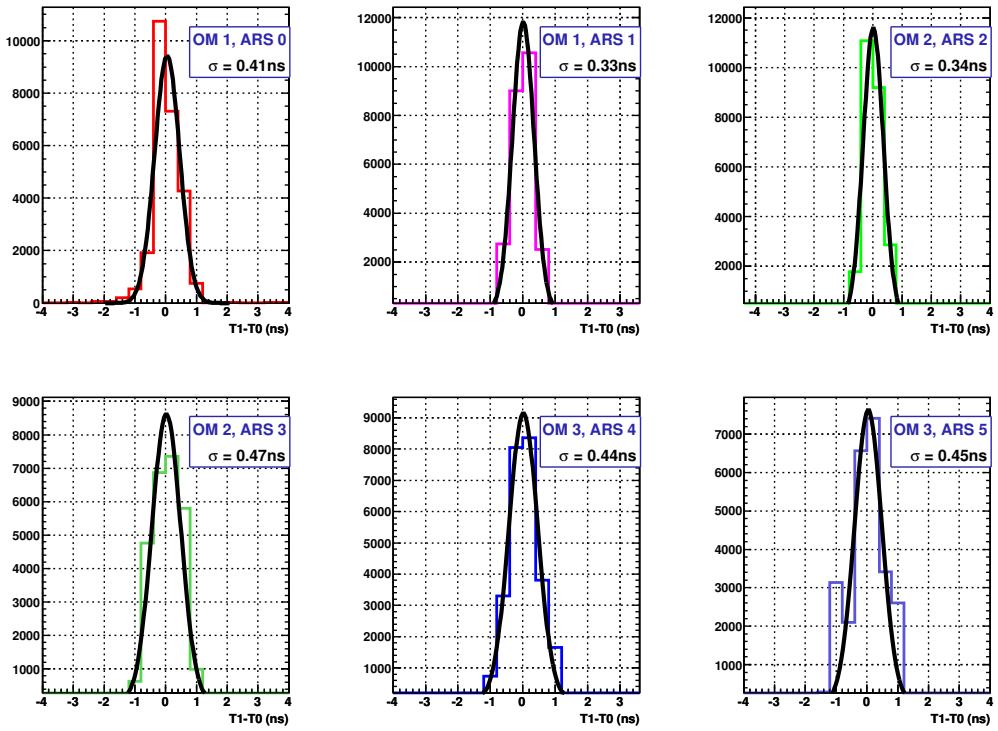

Fig. 8. Distribution of signal arrival times in the Optical Module (T1) with reference to the time of the LED Optical Beacon flash (T0). The measurement obtained by every ARS readout channel of the OM triplet is shown. Each distribution has been centered to 0 by subtracting its mean value before the fit of a Gaussian function. The resulting resolution value (σ) is indicated in each panel.

The complete timing resolution of the Optical Modules has been measured with the MILOM using the LED Optical Beacon system. As indicated in figure 1, an LED beacon is located in the bottom storey underneath the OM triplet of the second storey at a distance of about 15 metres. This beacon contains 36 individual blue LEDs ($\lambda = 470$ nm, dominant wavelength) syn-

chronised in time and arranged to give a quasi-isotropic light emission. A small PMT internal to the LED beacon monitors the output light pulse timing and amplitude and provides the time reference of the light flash.

The measurement of the OM timing resolution is performed by pulsing the LED beacon at a frequency of 30 Hz. Figure 8 shows the distribution of signal arrival times in the three OMs relative to the reference PMT in the LED Beacon. For every OM, the measurement obtained by both ARS readout channels are shown, since every front-end chip can potentially induce a different intrinsic electronics contribution to the timing. In the time distribution shown in figure 8, the contribution of the small PMT inside the LED beacon is small since it has a fast rise time of 0.8 ns, and so the measurement is dominated by the OM contribution. As can be seen from the distributions shown in figure 8, the timing resolution of all Optical Module readout channels is measured to be $\sigma \sim 0.4$ ns. This resolution is however obtained for large intensity light pulses and so is not dominated by the PMT transit time spread but by the intrinsic electronics resolution. A detailed analysis of the dependence of timing resolution on light intensity is required to separate the various contributions, but this result already shows that the complete electronics contribution is smaller than 0.5 ns as required.

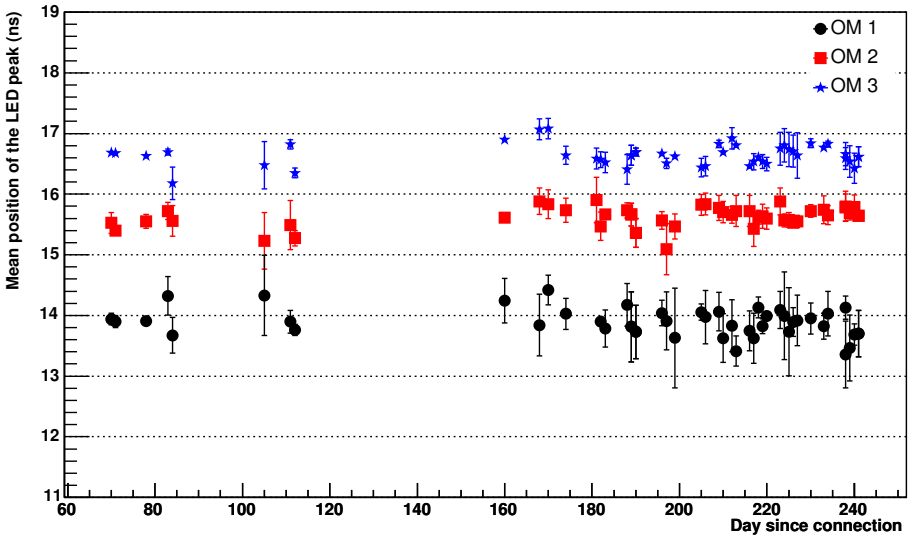

Fig. 9. Mean values of the arrival times of the OM signals induced by an internal LED flash with respect to the time of the flash. The mean time is displayed with reference to the start of the Time-to-Voltage converter (TVC) of the ARS. The plot displays the measurements obtained for the three OMs over a six month period. For every OM, the data points display the average value measured by its two ARS channels.

Every Optical Module also contains an internal blue LED in order to monitor the stability of the photomultiplier tube. This LED is mounted on the back of

the PMT, as shown in figure 2, and illuminates a large fraction of the photocathode through the phototube. The transit time of the PMT is monitored by flashing the internal LED at a rate of about 100 Hz and by looking at the OM signal arrival time with respect to the time of the LED flash. Figure 9 shows the average values of these delays for each of the three OMs as a function of time. The results confirm that the transit time of each OM has remained stable to within 0.5 ns, throughout the six month period considered.

5 Acoustic positioning system resolution

The second essential element to achieve the necessary angular resolution of the neutrino telescope is a real time measurement of the position in space of the Optical Modules with a precision of $\sim$ 10 cm. These positions are obtained by triangulation using distance measurements provided by the acoustic positioning system. The full acoustic positioning system will consist of a three dimensional array of emitting transducers (RxTx modules) fixed in known positions on the sea bed, together with receiving hydrophones (Rx modules) attached on several storeys along every detector line. These devices exchange precisely timed acoustic signals in the 40-60 kHz frequency range. In addition, the acoustic system includes four autonomous transponders which emit an acoustic "ping" at a precisely given frequency in response to a special interrogation by one RxTx module. These transponders will be located around the ANTARES detector in order to enlarge and make more uniform the geometry of the triangulation basis. At the present time, only a limited number of acoustic devices are installed at the site: one RxTx module on the MILOM anchor and one Rx module on its first storey. A first autonomous transponder has also been installed at the ANTARES site, its transducer being fixed at about 4 m above the sea bed on top of a pole supported by a pyramidal structure at a horizontal distance of $\sim$ 175 m from the MILOM anchor.

Although the limited number of installed acoustic emitters does not allow the triangulation reconstruction, the MILOM operation demonstrates the resolution and the stability of the acoustic system by monitoring the distance measured between two fixed points. This is illustrated in figure 10 which displays the acoustic distance measured between the RxTx transducer attached on the MILOM anchor and the autonomous transponder. The acoustic system measurements show a resolution of a few mm and a stability of $\sim$ 1 cm over a distance of 174.91 m, during two months of operation. The absolute distance obtained by this system is well in agreement with the value of 175.6 m obtained with the long base line acoustic navigation system used onboard the surface boat during the marine operation to monitor the deployment and installation of the lines. This navigation system, based on 10 kHz range acoustic signal exchanges, allows range measurements of several thousands of metres with an

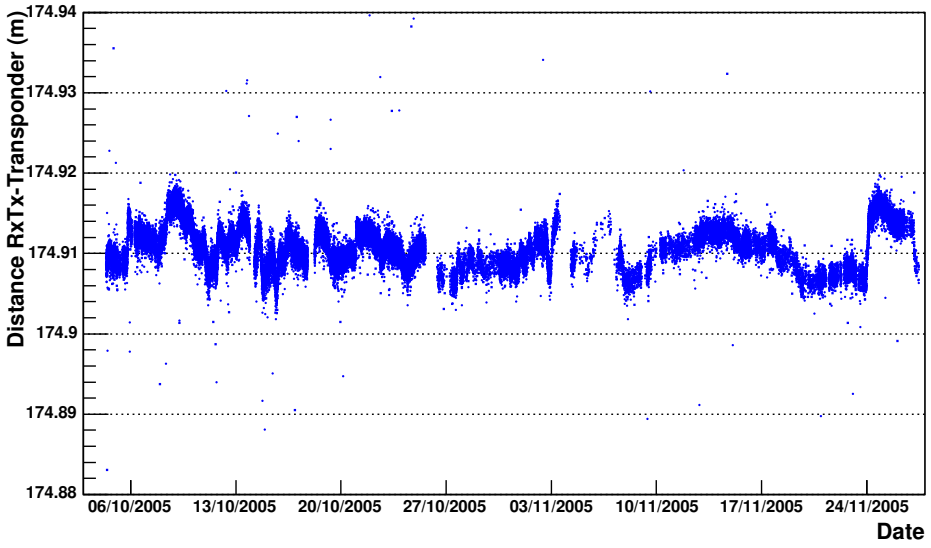

Fig. 10. Distance measured by the acoustic positioning system between the RxTx module and the autonomous transponder, both being fixed a few metres above the sea bed. The measurement is displayed as a function of time, during two months of operation.

accuracy limited to $\sim$ 1 m. With the MILOM operation, the performance of the acoustic positioning system is confirmed to be well within the specification required to obtain a precision of $\sim$ 10 cm on the spatial reconstruction.

6 Examples of instrumentation measurements

In parallel to the Optical Module data taking and to the operation of the calibration devices, the various instruments of the MILOM dedicated to environmental measurements have been regularly read out. This has allowed a continuous monitoring of some physical quantities of the sea water at the ANTARES site which might have an influence on the calibration of the detector or on the bioluminescence background: the water current flow; the water temperature; the sound velocity and the water transparency. As an example, the measured water current velocity recorded by the Doppler current profiler located on the MILOM top storey is displayed in figure 11, as a function of time over a period of eight months. These measurements confirm that the water current usually remains small at the ANTARES site, with a velocity not exceeding 20 cm/s and with an average speed of $\sim$ 5 cm/s.

Figure 12 shows the individual headings of the three storeys of the line measured by the compass in each electronics container, as a function of time for the same period. Although each storey has its own relative orientation due

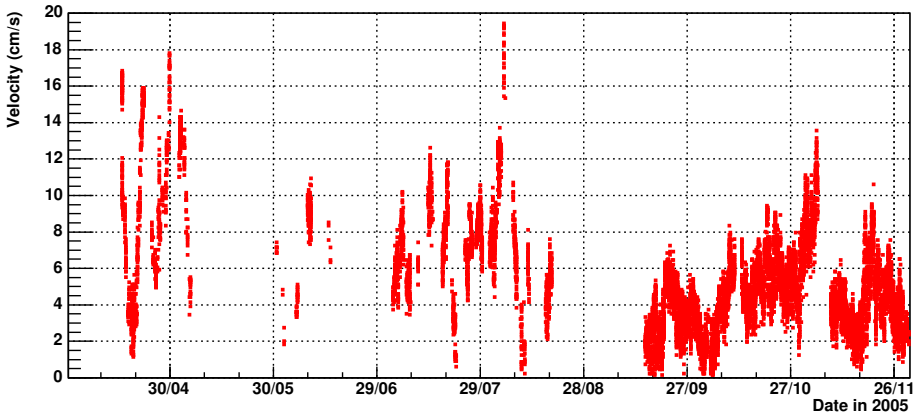

Fig. 11. Velocity of the water current flow measured by the Doppler current profiler, as a function of time over a period of eight months.

to the uncontrolled alignment in construction, the rotation changes affect, in general, the whole line. As expected, the top storey shows a larger rotation amplitude than the others. The measurements also indicate that the two lower storeys, separated by a shorter cable of 12.5 m, tend to remain at a constant orientation with respect to each other. Some correlation between the storey rotations and the water direction changes can also be noticed, especially when the current velocity is large as during the first days of November 2005.

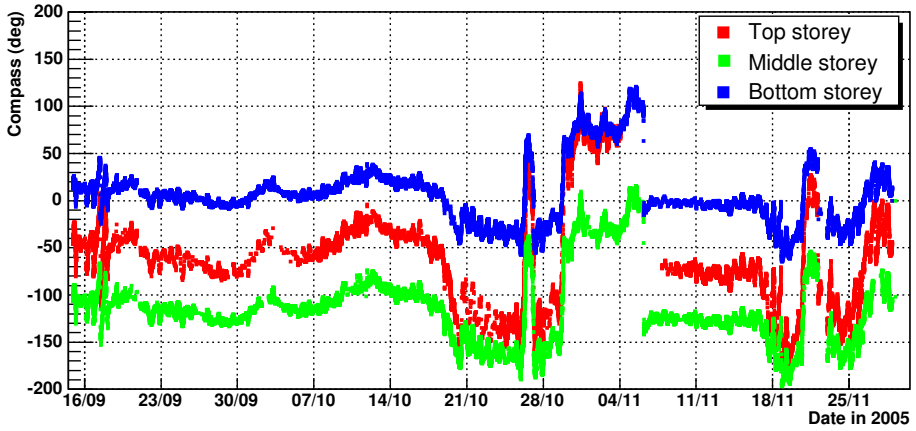

Fig. 12. Individual headings of the three MILOM storeys, measured by the compass included in every electronics container, as a function of time during two months of monitoring.

The seismometer read out by the MILOM has been delivering continuous data to the ANTARES shore station. It provided clear signals from several earthquakes around the world, such as the one in Japan on August 30^{th} 2005 and in Peru on September 24^{th} 2005. Further analyses of the seismometer data are in progress.

7 Conclusions

Since April 2005, the ANTARES Collaboration has been operating a Mini Instrumentation Line equipped with Optical Modules immersed at a depth of 2500 m on the ANTARES site. The main purpose of this line, built with pre-production elements of the detector, was to allow an in-situ check of all the equipment and in particular to validate the performance of the time calibration and acoustic positioning devices.

The various data regularly acquired during the MILOM operation confirm the capability of the Optical Modules and of its front-end electronics to trigger and read out single photo-electron signals. The continuous data collection from the OMs and the MILOM instruments during several months validate the whole electronics and the DAQ readout system designed for the detector. The operation of the light source calibration devices, such as the LED Optical Beacon or the OM internal LED, shows that a time calibration of all Optical Modules can be achieved in-situ with an accuracy better than 0.5 ns. The results yield an electronics contribution to the OM timing resolution smaller than 0.5 ns, as required. Finally, the operation of the acoustic positioning system shows that its performance is well within the specification required to achieve a space resolution of ~ 10 cm. All these results confirm the good performance of the electronics and calibration devices as required to obtain the desired angular resolution of the detector. The experience with the MILOM gives confidence for the operation of the first complete lines of the ANTARES neutrino telescope, the deployment of which has started in early 2006.

Acknowledgements

The authors acknowledge the financial support of the funding agencies. In particular: Centre National de la Recherche Scientifique (CNRS), Commissariat à l'Énergie Atomique (CEA), Commission Européenne (FEDER fund), Région Alsace (contrat CPER), Région Provence-Alpes-Côte d'Azur, Département du Var and Ville de La Seyne-sur-Mer, in France; Bundesministerium für Bildung und Forschung (BBF), in Germany; Istituto Nazionale di Fisica Nucleare (INFN), in Italy; de stichting voor Fundamenteel Onderzoek der Materie (FOM) and the Nederlandse organisatie voor Wetenschappelijk Onderzoek (NWO), in the Netherlands; Russian Foundation for Basic Research (RFBR), in Russia; Ministerio de Educación y Ciencia (MEC), in Spain.

References

[1] E. Aslanides et al., ANTARES Collaboration, the ANTARES Proposal, astro-ph/9907432.

[2] P. Amram et al., ANTARES Collaboration, Nucl. Inst. Meth. A 484 (2002) 369 (astro-ph/0112172).

[3] J.A. Aguilar et al., ANTARES Collaboration, Nucl. Inst. Meth. A 555 (2005) 132 (physics/0510031).

[4] V. Bertin on behalf the ANTARES Collaboration, "Status of the ANTARES neutrino detector", 8th International Workshop on "Topics in Astroparticle and Underground Physics" (TAUP 2003), proceed. suppl. Nucl. Phys. B 138 (2005) 195.

[5] J.A. Aguillar et al., ANTARES Collaboration, Astropart. Phys. 23 (2005) 131 (astro-ph/0412126).

[6] P. Amram et al., ANTARES Collaboration, Astropart. Phys. 19 (2003) 253 (astro-ph/0206454).

[7] D. Lacharte and F. Feinstein on behalf of the ANTARES Collaboration, "Application Specific Integrated Circuits for Antares Offshore Front-end Electronics", 2nd International Conference on "New developments in Photodetection" (Beaune 1999), proceed. suppl. Nucl. Inst. Meth. A 504 (2003) 258.

[8] P. Amram et al., ANTARES Collaboration, Astropart. Phys. 13 (2000) 127 (astro-ph/9910170).